ADVANCES IN ATMOSPHERIC SCIENCES, VOL. 33, MARCH 2016, 339–351

Assessment of Interannual Sea Surface Salinity Variability and Its Effects on the Barrier Layer in the Equatorial Pacific Using BNU-ESM

Hai ZHI[1], Rong-Hua ZHANG[*2], Fei ZHENG[3], Pengfei LIN[4], Lanning WANG[5], and Peng YU[6]

[1]*Earth System Modeling Center and College of Atmospheric Sciences, Nanjing University of Information Science and Technology, Nanjing* 210044

[2]*Key Laboratory of Ocean Circulation and Waves, Institute of Oceanology, Chinese Academy of Sciences, Qingdao* 266071

[3]*International Center for Climate and Environment Science, Institute of Atmospheric Physics, Chinese Academy of Sciences, Beijing* 100029

[4]*State Key Laboratory of Numerical Modeling for Atmospheric Sciences and Geophysical Fluid Dynamics, Institute of Atmospheric Physics, Chinese Academy of Sciences, Beijing* 100029

[5]*College of Global Change and Earth System Science, Beijing Normal University, Beijing* 100875

[6]*Cooperative Institute for Climate and Satellites, University of Maryland, College Park, MD* 20740, *USA*

(Received 11 July 2015; revised 2 September 2015; accepted 28 September 2015)

ABSTRACT

As salinity stratification is necessary to form the barrier layer (BL), the quantification of its role in BL interannual variability is crucial. This study assessed salinity variability and its effect on the BL in the equatorial Pacific using outputs from Beijing Normal University Earth System Model (BNU-ESM) simulations. A comparison between observations and the BNU-ESM simulations demonstrated that BNU-ESM has good capability in reproducing most of the interannual features observed in nature. Despite some discrepancies in both magnitude and location of the interannual variability centers, the displacements of sea surface salinity (SSS), barrier layer thickness (BLT), and SST simulated by BNU-ESM in the equatorial Pacific are realistic. During El Niño, for example, the modeled interannual anomalies of BLT, mixed layer depth, and isothermal layer depth, exhibit good correspondence with observations, including the development and decay of El Niño in the central Pacific, whereas the intensity of the interannual variabilities is weaker relative to observations. Due to the bias in salinity simulations, the SSS front extends farther west along the equator, whereas BLT variability is weaker in the central Pacific than in observations. Further, the BNU-ESM simulations were examined to assess the relative effects of salinity and temperature variability on BLT. Consistent with previous observation-based analyses, the interannual salinity variability can make a significant contribution to BLT relative to temperature in the western-central equatorial Pacific.

Key words: feedback, interannual variability, sea surface salinity, barrier layer thickness

Citation: Zhi, H., R.-H. Zhang, F. Zheng, P. F. Lin, L. N. Wang, and P. Yu, 2016: Assessment of interannual sea surface salinity variability and its effects on the barrier layer in the equatorial Pacific using BNU-ESM. *Adv. Atmos. Sci.*, **33**(3), 339–351, doi: 10.1007/s00376-015-5163-y.

1. Introduction

It is well known that ENSO is Earth's dominant source of interannual climate variability in the tropical Pacific. Extensive studies have confirmed that ENSO originates from air–sea interactions in the equatorial Pacific (e.g., Maes et al., 2006). Furthermore, the oceanic thermal structure of the Pacific warm pool has been found to be tightly related to the evolution of ENSO events (e.g., McPhaden and Picaut, 1990). Although this effort has improved our understanding of ENSO physics, considerable attention has recently been paid to the salinity variability and its effects on SST anomalies in the tropical Pacific. In particular, salinity and the related freshwater flux have a strong effect on the stratification stability in the upper ocean, leading to a feedback effect on the interannual variability associated with ENSO (Zhang et al., 2010; Zheng and Zhang, 2015).

In addition to temperature, salinity is another important physical field of the ocean that controls its dynamic and thermodynamic behaviors (Godfrey et al., 1995). For example, the salinity can strongly stratify the near-surface region and reduce the response time of SST to surface fluxes in areas with excessive precipitation (Rao and Sivakumar, 2003). The deep mixed layer (ML) of temperature along with strong salinity stratification leads to the necessary conditions for

* Corresponding author: Rong-Hua ZHANG
Email: rzhang@qdio.ac.cn

the formation of the barrier layer (BL) (Mignot et al., 2009). Thus, the vertical structure of salinity also contributes to the formation of the near-surface ML and its dynamics (Lukas and Lindstrom, 1991; Sprintall and Tomczak, 1992). For example, Lukas and Lindstrom (1991) found that a systematic difference exists between the bottom of the isothermal layer (IL) and the top of the ML due to salinity stratification; this intermediate layer is referred to as the BL, which is located between the base of ML and the top of the thermocline. By insulating the surface water from the colder deep ocean, the BL serves to inhibit the entrainment of the cold water below into the ML. The BL exhibits pronounced interannual variability, with its variation in thickness and occurrence rates differing among the oceans and seasons (Sato et al., 2006).

In the western Pacific, a BL is formed in the IL when the subduction of warm and salty water occurs from the South Equatorial Current beneath fresh and warm pool water (Lindstrom et al., 1987; Lukas and Lindstrom, 1991; Maes et al., 2005, 2006). Observations indicate that a thick BL is present on the western side of the SSS front, moving back and forth along the equator. The relationship between the BL and air–sea interaction events (i.e., El Niño events) has recently been demonstrated (e.g., Vialard and Delecluse, 1998; Masson et al., 2004; Maes et al., 2006; Zheng et al., 2014; Zheng et al., 2015). Furthermore, Zhu et al. (2014) found that salinity anomalies can play a vital role in its evolution, as well as in predicting the La Niña condition of 2007. Additionally, it has been shown that a BL near the date line induced by interannual salinity anomalies can significantly affect the temperature in the upper ocean (Zheng et al., 2014), serving to enhance ENSO. For example, during El Niño, westerly winds drive the warm pool eastward, allowing fresh water to ride on top of the local colder/saltier/denser water to the east. In fact, the BL near the date line caused by the interannual salinity anomalies can significantly affect the temperature fields in the upper ocean, indicating positive feedback (Zhang and Busalacchi, 2009). Warm water buildup is evident, as indicated by a large BL thickness (BLT) in the western equatorial Pacific, initiating El Niño development (Yim et al., 2008); on the contrary, during the onset of El Niño, the removal of the BL can reduce or abort El Niño, as demonstrated in a coupled model (Maes et al., 2002). Later studies confirmed the relationship between the eastward migration of the warm pool during El Niño and BL heat storage in the western Pacific (Mignot et al., 2009). This helps discharge the heat stored in the thick BL in the western equatorial Pacific (Maes and Belamari, 2011). Then, in the central equatorial Pacific, the interannual variations of the BL almost co-vary with ENSO, and the lead time is about two months with respect to those of the local SST (Zheng et al., 2014). It was concluded that the presence of a BL significantly affects heat entrainment into the ML, thereby impacting the SST and, consequently, ENSO variability (Bosc et al., 2009). This needs to be adequately represented in climate models to capture ENSO properties.

Currently, coupled ocean–atmosphere models are able to reproduce the salinity effect on SST, as well as the potential resulting feedback. To study this feedback mechanism or for forecasting purposes, for example, a hierarchy of models has been designed. These models include intermediate complexity models (e.g., Zhang et al., 2005), hybrid coupled models (e.g., Zhang and Busalacchi, 2009), and Coupled General Circulation ModelsCGCMs (e.g., AchutaRao and Sperber, 2006; Zhu et al., 2013). Currently, there is high confidence that CMIP5 multi-models are able to capture the main physical processes during transient ocean heat uptake, along with coupled modes of low-frequency variability (IPCC, 2013). It is essential that salinity stratification be carefully considered in climate modeling and forecasts and that the feedback processes at work contain a fully coupled response of the ocean–atmosphere system. Despite progress in simulating SST and basic ENSO features in the equatorial Pacific, the coupled models from CMIP5 have struggled with realistic simulations compared with CMIP3 (Bellenger et al., 2014). These coupled models in particular display a large range of ENSO amplitude, and the variability center extends too far into the western Pacific (Yu and Kim, 2010). Some reasons for these biases have been proposed, such as a too diffusive thermocline, deficient horizontally isotropic mixing coefficients, and excessive/insufficient rainfall (Guilyardi et al., 2009; Yu and Kim, 2011; Su and Jiang, 2012). Furthermore, the warm water of the so-called warm pool in the western equatorial Pacific is misrepresented in most of the CGCMs (Maes et al., 2005). In addition to complex interactions among the ocean processes, it is difficult to identify the ultimate source of these errors (Vannière et al., 2011). The BL may play a role in inducing ENSO simulation biases, but this has not been fully investigated in the tropical Pacific.

The intention of the present study was to specifically evaluate the salinity interannual variability and its impact on the BL in the equatorial Pacific using outputs from BNU-ESM. Because a process-based model evaluation can help identify the cause of specific biases, the following questions were investigated: Can the interannual salinity variations of the tropical Pacific be realistically described by BNU-ESM? Can BNU-ESM reproduce the mechanisms of BL formation and its main contributions to interannual variability in the equatorial Pacific? Section 2 gives a brief description of BNU-ESM, as well as the observations and methods used in this study. Section 3 presents the main results and the simulation performance in terms of BLT interannual variability; the responses to ocean physical fields are analyzed by comparing the BNU-ESM simulations with observations, and the sensitivity of SSS to SST evolutions and the potential contributing factors to ENSO are diagnosed. A summary of the study's key findings is provided in the final section.

2. Model, data and analysis methodology

2.1. *BNU-ESM*

The structure and individual components of BNU-ESM are briefly described as follows; a more comprehensive description can be found in Ji et al. (2014). BNU-ESM is a fully-coupled earth system model. Using one central cou-

pler component (the improved NCAR-CPL6), BNU-ESM simultaneously consists of four separate models to simulate the Earth's atmosphere (CAM3.5), sea-ice (CICE4.1), land surface [BNU-CoLM3 (Common Land Model)] and ocean (MOM4p1). Two special processes included in BNU-ESM are an ecosystem–biogeochemical module [iBGC (The idealized ocean biogeochemistry module] in the ocean component and an atmospheric CO_2 concentration model fully coupled to land and ocean CO_2 fluxes. BNU-ESM has participated in CMIP5 and has provided future climate projections for IPCC AR5.

BNU-ESM's ocean output uses a nominal latitude–longitude resolution of 1° (downscaled to 1/3° within 10° of the tropical domain), with a 360° (lon) ×200° (lat) grid. There are 50 vertical levels, with the uppermost 23 layers each having a depth of approximately 10 m. The atmospheric output uses an Eulerian dynamical core for transport calculations, with a T42 horizontal spectral resolution ($2.81^\circ \times 2.81^\circ$ horizontal grid, approximately) and 26 levels in the vertical direction.

For this paper, we selected the last 100 years (model years 1450 to 2008) of the pre-industrial control simulation to examine the characteristics of mean climatology and interannual variability (Taylor et al., 2012). The model outputs used include ocean temperature, salinity etc.

2.2. *Observational data*

The 3D gridded data of temperature and salinity are from the Array for Real-Time Geostrophic Oceanography (ARGO) products (Roemmich et al., 2009), which include monthly and long-term climatological mean fields spatially averaged within 1° bins at standard depths. The same as those used for the World Ocean Atlas (Levitus, 1982), the ARGO products have 26 vertical (standard) levels in the upper 2000 m and span from January 2005 to present. The above data sets were regridded as required onto a common $1^\circ \times 1^\circ$ grid using bilinear interpolation.

2.3. *Methodology*

Ocean temperature and salinity were used to estimate potential density, MLD, ILD, and BLT. The potential density was calculated using the standard routine in Gill (1982), and the MLD (ILD) was calculated as the depth where the density (temperature) is $\Delta\rho$ higher (ΔT lower) than that at 10 m depth, where $\Delta T = 0.2^\circ$C and $\Delta\rho = -(\partial\rho/\partial T)\Delta T$. The BLT was defined as in de Boyer Montégut et al. (2004) and Bosc et al. (2009), which is the difference between the MLD and ILD when the MLD is shallower than the ILD.

To identify the effective contributions of temperature and salinity to BLT, Zheng and Zhang (2012) proposed a diagnostic method with which the relative effects of climatologically or interannually varying temperature and salinity fields can be evaluated in an interannual anomaly field of interest (Table 1). The diagnostic results were then used to distinguish the contributions of interannual variations of temperature and salinity to BLT.

Table 1. Methods by which interannual BLT variability is calculated in terms of temperature and salinity fields, which can be considered to be either interannually varying or climatologically varying.

Name of calculated field	Dependence on the variabilities of temperature and salinity used
BLT ($T_{\text{clim}}, S_{\text{clim}}$)	Both climatologically varying temperature and salinity fields
BLT ($T_{\text{inter}}, S_{\text{inter}}$)	Both interannually varying temperature and salinity fields
BLT ($T_{\text{inter}}, S_{\text{clim}}$)	Interannually varying temperature and climatological salinity
BLT ($T_{\text{clim}}, S_{\text{inter}}$)	Climatological temperature and interannually varying salinity

3. Analysis and assessment

3.1. *SST interannual variability and related oceanic fields*

Because of the study's focus on the upper ocean salinity effects on interannual variability, a preliminary assessment was required to analyze the spatial pattern of SSS, BLT and SST interannual anomalies in the equatorial Pacific. The spatial distributions of interannual anomalies simulated by BNU-ESM were explored in the tropical Pacific and compared with observations (Fig. 1). The spatial distributions of the SSS, BLT and SST interannual variability observed in the equatorial Pacific indicate a maximum variability of SSS that occurs in the western equatorial Pacific, whereas a BLT maximum variability is seen near the equator between 160°E and the date line. Correspondingly, an SST maximum variation appears in the central-eastern equatorial Pacific. At these locations, the variabilities are large, with standard deviations up to 0.4 psu, 8 m and 0.8°C for SSS, BLT and SST variabilities, respectively. The BL is instrumental in maintaining heat and momentum in the warm pool within the salinity stratified layers, which is generally consistent with the results from previous studies (Picaut et al., 1996; Delcroix and Picaut, 1998; Stoens et al., 1999).

BNU-ESM can reasonably well reproduce the general features of the relationships among SSS, BLT and SST interannual variability in spatial distribution terms (Figs. 1d–f), in spite of biases in magnitude. SSS and BLT interannual variability simulated in the western tropical Pacific are stronger than observed (Figs. 1g and h), whereas a larger SST interannual variability is observed in the eastern tropical Pacific (Fig. 1l). However, in the western tropical Pacific, the marked difference is that SSS and BLT interannual variability relationships tend to be opposite in the BNU-ESM simulations compared with observations. Additionally, an SST difference (amplitude of 1°C) exists in the eastern equatorial Pacific, which is 0.4°C–0.8°C larger than observed (Fig. 1i). The SST sensitivity to SSS simulated by BNU-ESM also indicates the influence of SSS on SST in the equatorial Pacific.

Figure 2 shows the temporal evolutions of SSS, BLT and SST interannual variability across the equatorial Pacific. With its spatiotemporal displacement, the largest SST

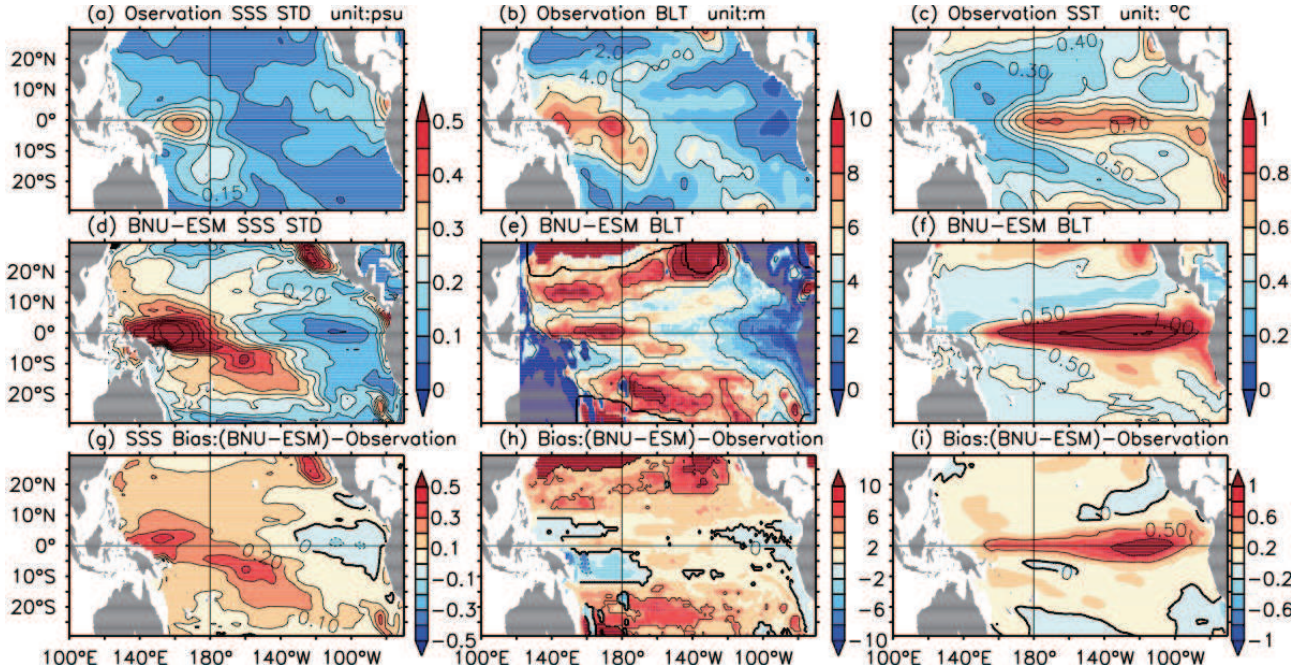

Fig. 1. Horizontal distribution of the standard deviation (STD) of ocean fields in the equatorial Pacific simulated by BNU-ESM and ARGO data: (a–c) SSS, BLT and SST STD from the observation; (d–f) SSS, BLT and SST STD simulated by BNU-ESM; (g–i) difference between the BNU-ESM simulations and ARGO data. The units are psu for SSS, °C for SST, and m for BLT.

variability occurs in the central-eastern equatorial Pacific, whereas large SSS variability is located in the western and central basin (Figs. 2a and b). The interannual SSS variability shows a standing feature in which the horizontal pattern is centered in the western-central equatorial Pacific around the date line, where a large freshwater flux variability occurs (e.g., Zhang and Busalacchi, 2009). For example, a large positive SST anomaly is located in the eastern and central equatorial Pacific, whereas its negative counterpart is located in the central and western basin during El Niño events. However, at the transition from El Niño to La Niña, the sea water is anomalously cold and salty in the central equatorial Pacific (Fig. 2b).

As shown in Fig. 2c, a distinctly interannual BLT anomaly exists in the equatorial Pacific. A zonal seesaw pattern of interannual BLT variations is evident along the equator. The BLT variability is different between the 130°–160°E and 160°E–170°W areas in the tropical Pacific. In a previous observational study, Delcroix et al. (2011) revealed that the BL is anomalously thin (thick) west of 160°E, but thick (thin) in the east, during El Niño (La Niña).

As evident in the longitude–time plots of the equatorial interannual SSS, BLT and SST anomalies simulated by BNU-ESM (Fig. 3), a large SSS variability lies in the central and western equatorial Pacific (Fig. 3a), whereas a large SST variability appears in the eastern and central basin (Fig. 3b). Additionally, the interannual BLT variations show a distinct horizontal pattern centered around the date line in the western-central equatorial Pacific (Fig. 3c). BNU-ESM reproduces the observed interannual feature in which a negative/positive SSS anomaly corresponds to a positive (negative) BLT in the central-western equatorial Pacific, leading to a warmer (cooler) SST in the central-eastern equatorial Pacific during ENSO cycles. Compared with observations, variabilities in both the SSS and precipitation simulated by BNU-ESM are greater in the western equatorial Pacific (Ji et al., 2014). The biases are mainly due to a smaller climatological mean simulated by BNU-ESM (Zhi et al., 2015). Another difference is that the regions with large SSS and BLT anomalies in the western equatorial Pacific extend farther east across the date line than observed. Hence, these biases result in a greater SST amplitude, with a large SST anomaly extending farther west across the date line than observed in the equatorial Pacific. These biases are related to the spatial distribution of the SSS interannual anomalies simulated by BNU-ESM, where the simulated SSS structure is quite sensitive to freshwater forcing and other fluxes (Vialard and Delecluse, 1998).

3.2. *Interannual variability in BLT*

From the above analyses and the work of Zheng et al. (2014), there are two evident regions in which ENSO evolves differently in the equatorial Pacific: the western zone (130°–160°E) and eastern zone (160°E–170°W). As mentioned in the introduction, a significant BLT interannual variability primarily results from salinity and temperature interannual variations in the equatorial Pacific through their impact on the ILD and MLD.

As shown in Fig. 4a, the BL, ML and IL in the western zone (i.e., 130°–160°E) present near opposite values between ENSO simulations and observations. Compared to the BL's contribution to the onset of ENSO events in the western region, the BL varies almost synchronously with the observed

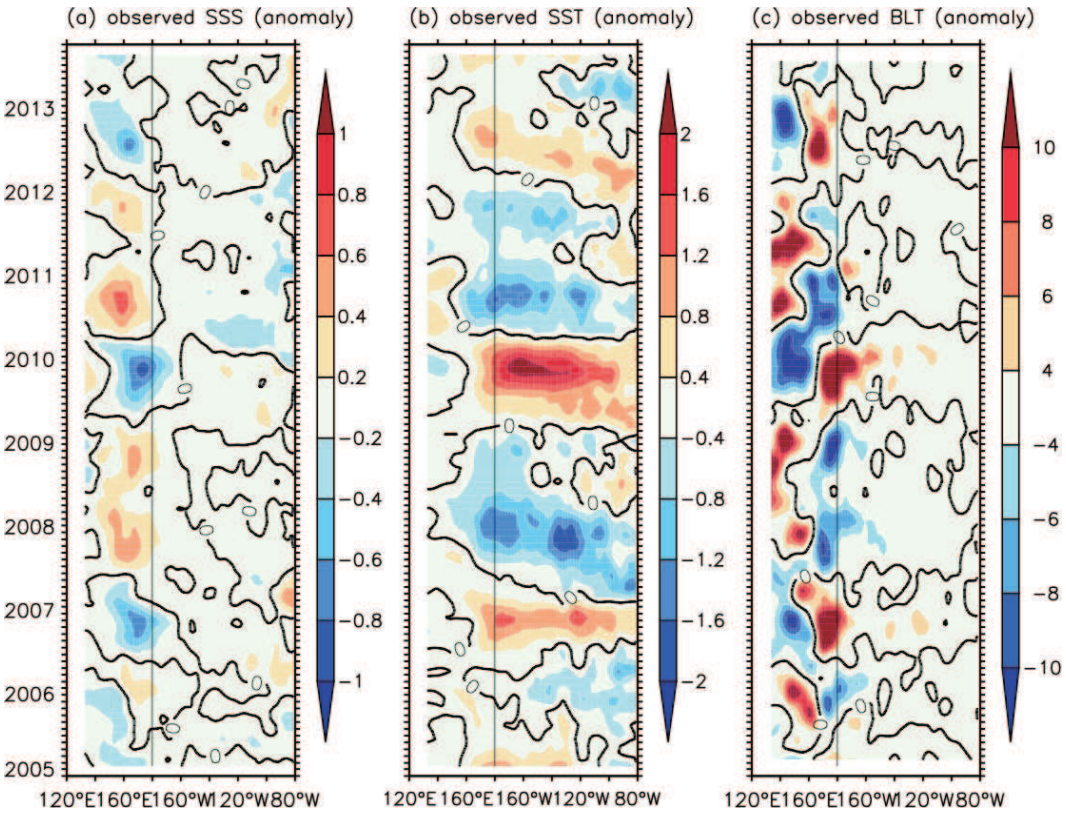

Fig. 2. Longitude–time sections along the equator (averaged between 2°N and 2°S) for (a) SSS, (b) SST and (c) derived BLT interannual anomalies observed from ARGO data for 2005–13. The contour interval is 0.2 psu in (a), 0.4°C in (b), and 2 m in (c).

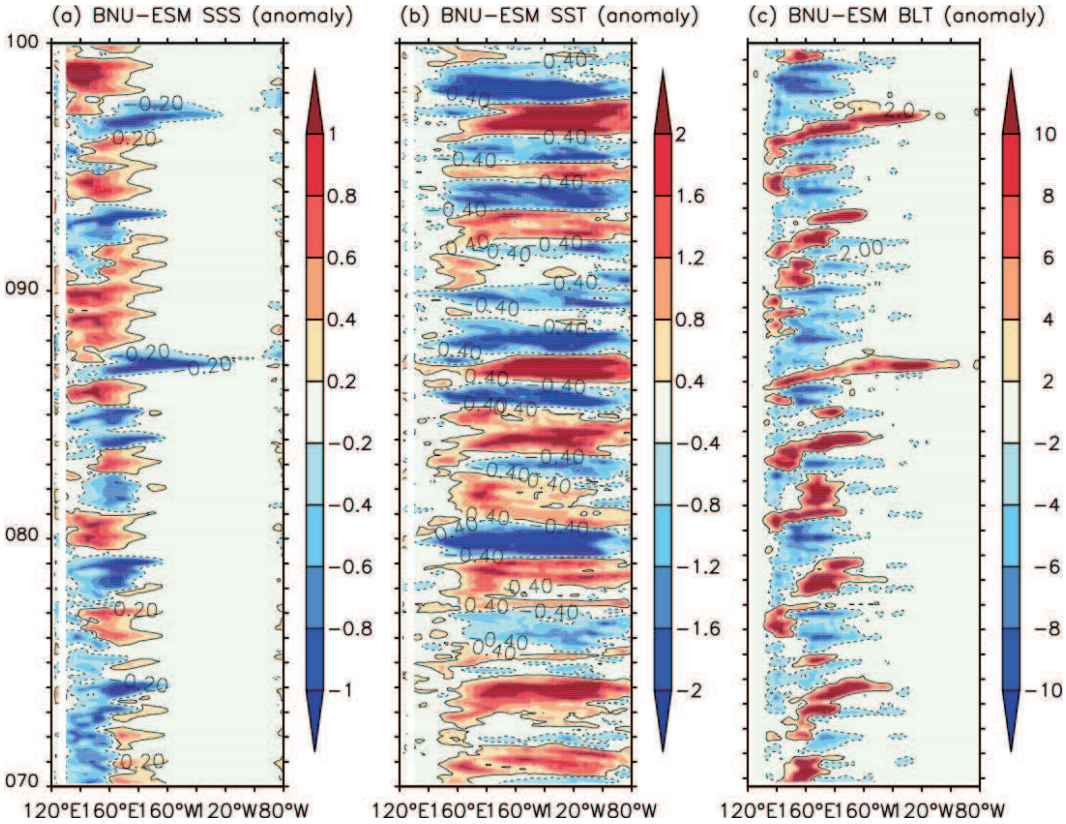

Fig. 3. As in Fig. 2 but for the interannual anomalies of (a) SSS (psu), (b) SST (°C), and (c) derived BLT (m) simulated by BNU-ESM. The *y*-coordinates are the last 30 years of 100 model years.

ENSO and becomes slightly thicker during El Niño events in the central part (i.e., 160°E–170°W). Furthermore, in the eastern part of the central equatorial Pacific, the main causes of BL interannual changes are the interannual variations of the MLD and ILD (Fig. 4b).

BNU-ESM captures how the BLT in the central basin varies almost synchronously with ENSO (Fig. 5). From the temporal variations of the ILD, MLD and BLT in the eastern zone (i.e., 160°E–170°W) simulations, the comparisons between the BNU-ESM simulation and observation show some differences in the amplitude of the interannual variability in the western part and the central part. For example, all vari-

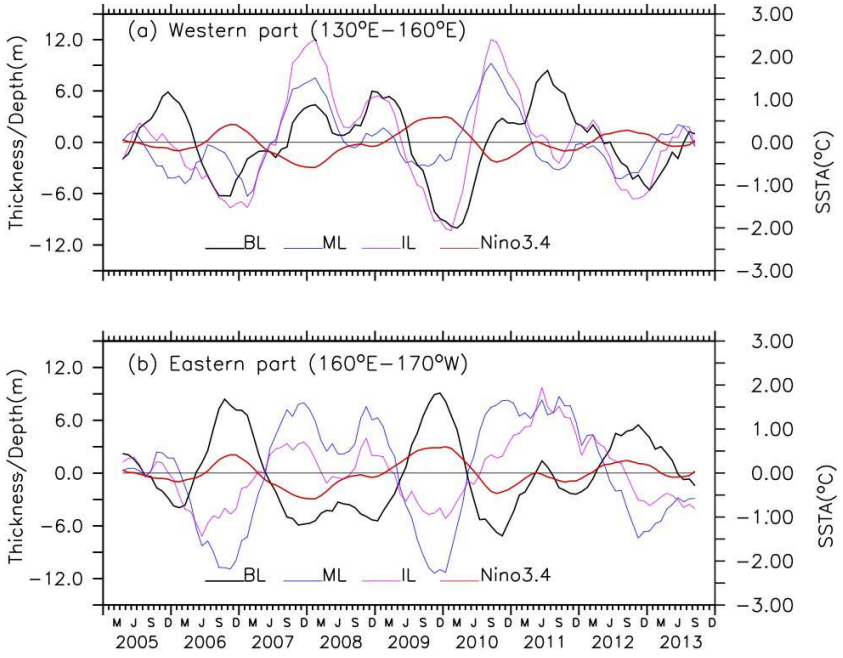

Fig. 4. Time series averaged in (a) the western part (2°S–2°N, 130°–160°E) and (b) the eastern part (2°S–2°N, 160°E–170°W) of the western-central equatorial Pacific for some derived fields observed from ARGO data: anomalous thickness of the BL (black line); anomalous depth of the ML (blue line) and IL (pink line); and Niño3.4 index (red line).

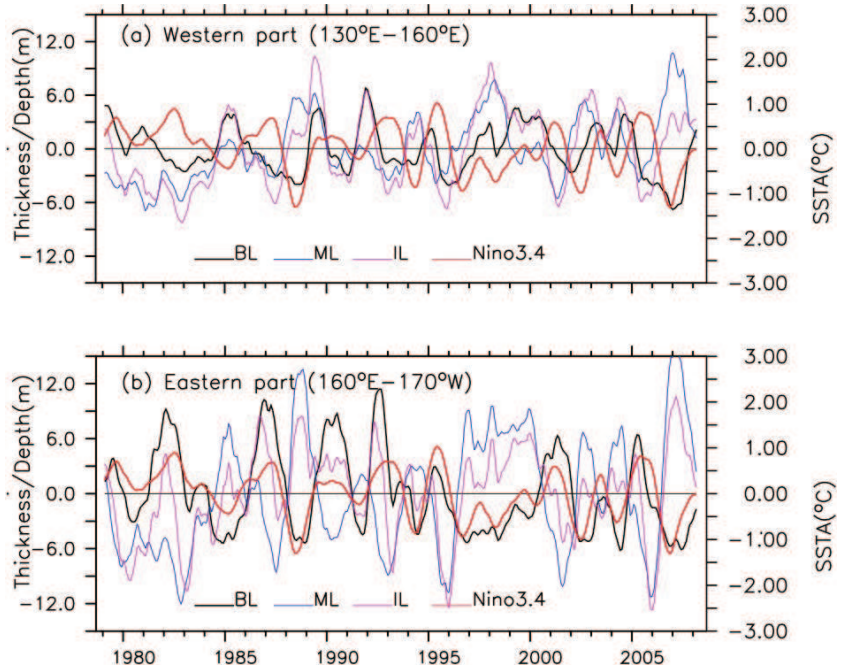

Fig. 5. As in Fig. 4 but for some derived fields simulated by BNU-ESM.

abilities in the western part, including the BLT, MLD and ILD, are weaker than that of the observation, with the weakest being the BLT anomaly. In the eastern part, BLT variability is slightly stronger than that observed during El Niño, which may be one reason why the simulated SST is larger than the observed SST.

3.3. *BLT evolution during ENSO*

In this next part of the study, the evolutions of the BLT, ILD and MLD during a composite ENSO event were explored and assessed. A particular focus was on the key mechanism that controls the formation, growth and decay of the BL. The warm phase of ENSO, El Niño, was selected for the analysis and evaluation of the evolutions of the BLT, MLD and ILD interannual anomalies and their relationships with SSS. Using the ARGO data, the years 2006 and 2009 were El Niño years, with the anomaly for three consecutive months being larger than 0.5°C. Using the BNU-ESM simulation, El Niño was defined as an anomaly larger than 0.8°C, meaning there were six El Niño events during the last 30 years of output. Figure 6 shows the longitude–time distribution of the 2°N–2°S averaged BLT, MLD and ILD for the El Niño composite event, both observed and simulated by BNU-ESM. The notation (−1), (0) and (+1) represents an El Niño "normal year", "developmental year" and "decay year", respectively. Months are represented by their three-letter abbreviations (Jan, Feb, Mar etc.).

For a normal year (Fig. 6a), a zonal BLT thicker than 20 m is maintained between 150°E and 170°E from Jan(−1), about one year ahead of the peak of El Niño. The BL in-

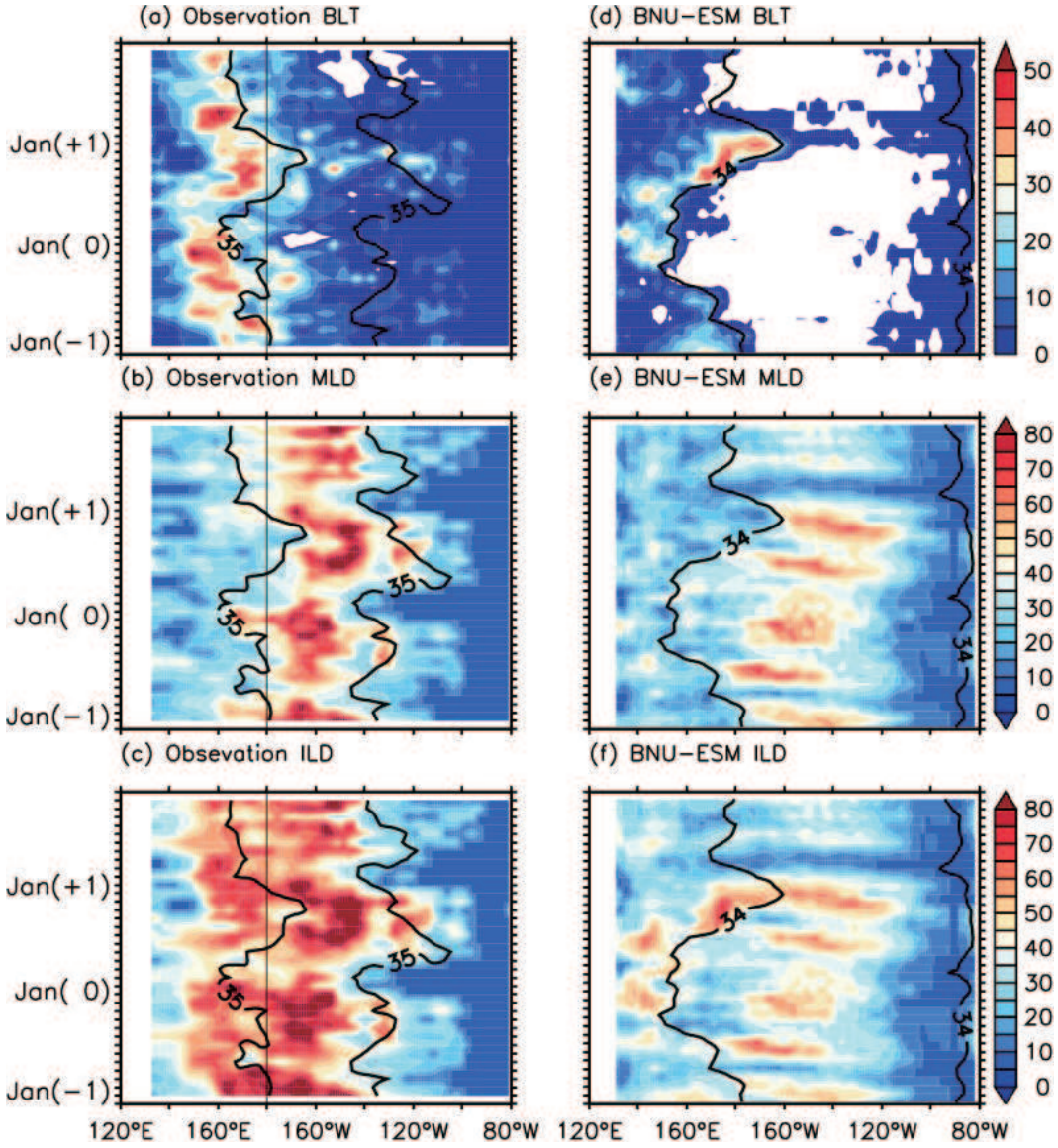

Fig. 6. Longitude–time distributions along the equator (averaged from 2°N to 2°S) of (a) BLT, (b) MLD and (c) ILD observed from ARGO during El Niño, and (d) BLT, (e) MLD and (f) ILD simulated by BNU-ESM. The units are m for the ILD, MLD and BLT. The black line of the 34 isohaline represents the SSS front for the observation; the black line of the 35 psu of the isohaline represents the SSS front simulated by BNU-ESM.

creases to above 30 m in the western region from Aug(0) and shifts to the east in the following months until it reaches its easternmost position from Oct(0) to Dec(0). As a result, a thick BL region is well extended in the central equatorial Pacific, and large BLTs (∼40 m) are spread westward to the date line. Then, after the peak of El Niño from Jan(1) to Feb(1), the BLT decreases slightly and shrinks westward due to El Niño decay. The region with the thick BL then disappears in less than 3 months. The shifting of the thick-BL region is strongly associated with the maximum zonal SSS gradient [black line: hereafter, 34.6 psu (observed) and 35.0 psu (simulated)], which is located in the east and limited by the maximum zonal SSS gradient. Here, the maximum zonal SSS gradient closely follows the 34.6 psu isohaline in the observed SSS, averaging between 2°S and 2°N, similar to the definition proposed by Zheng et al. (2014). This criterion indicates an exact boundary to the eastern edge of the warm pool (Brown et al., 2014). An important conclusion can thus be verified: a thick-BL region exists from the eastern edge of the warm pool to the west of this border. As seen above, the BLT interannual variability is an indicator of the evolution of an El Niño event.

By definition, analysis of the composite evolution of the MLD and ILD explains, to some extent, the evolution of the BLT. Figure 6b exhibits a region of quasi-permanent large MLD (>50 m) at 170°–130°W during the beginning of year(−1) and the middle of year(0). It is important to note that the SSS front appears as a relatively sharp border, whereas the region of thin MLD (<40 m) separates to the west and the thick MLD (>50 m) extends to the east. Hence, the eastward displacement of the large MLD region from Aug(0) is associated with the eastward displacement of the SSS front. From Dec(0) to Feb(1), the western edge of the large MLD region moves westward, whereas the SSS front retreats westward. Note that the MLD in the east of the SSS front is 70–80 m from the peak [Oct(0) to Jan(1)] until the end of El Niño.

Figure 6c illustrates that a region with an ILD quasi-permanent deep IL (>50 m) appears in the central Pacific, compared to the large MLD region that extends farther east. The 34.6 psu contour does not sharply border the region with the ILD deep IL, and an ILD (>50 m) sometimes exists up to 20°–30° longitude west of the 34.6 psu contour. The ILD in the central Pacific increases from the middle of year(0). From Jan(1) to Mar(1), the ILD does not deepen as much as in the two previous years, and it remains shallow for the rest of the year, similar to the MLD feature.

Compared with the shifting of the MLD and ILD along the equatorial Pacific, the thick BL appears toward the west of the SSS front only. Both the ML and IL are deep at roughly the same depth in the east of the warm pool, leading to a very thin BL. However, there is a contrasting change in the IL and ML to the west of the eastern edge of the warm pool. This mechanism is such that growth and decay are highly related to the displacement of the ILD. When El Niño develops, a positive heat content anomaly appears to result in a deeper ILD and leads to the thickening of the BL. BLT variation is thus closely associated with the same variability as the ILD anomalies in the warm pool.

Compared with observations, BNU-ESM effectively reproduces the evolving features of the BLT, MLD and ILD interannual anomalies and their relationships with SSS during El Niño, with the large variabilities moving back and forth across the SSS front along the equator during ENSO (Figs. 6d–f). For example, a zonal BLT is permanently maintained to the west of 160°E, even though the simulated BLT is thinner than the observed BLT. Additionally, the BLT increases by at least 30 m in the western region and extends eastward from Oct(0), two months later than that observed. However, the duration of a large BLT (over 30 m) is approximately 3 months, much shorter than that observed in the El Niño developing phase. The simulated evolutions of the BLT, MLD and ILD and their shift along the equator are both weaker than those observed.

Although the simulated salinity value of the SSS front representing the maximum zonal SSS gradient (35 psu) is higher than observed (34.6 psu), it realistically reproduces the movement along the equator and the variations in intensity. Due to the higher simulated SSS interannual variability in the western equatorial Pacific, the SSS front moves eastward in Feb(0), 2 months earlier than observed, whereas a large BLT (∼30 m) forms in the western equatorial Pacific and moves eastward. Similar to the MLD, the ILD in Jan(1) to Mar(1) is shallower than observed during previous years, and remains shallow compared to the previous years. At 150°–170°E, the BLT is associated with the ILD in combination with a near constant MLD in Jan(0). The region with the thick BL is also zonally larger than observed in Jan(1) because the simulated eastward shift of the thickened ILD is less significant than that of the warm pool at the onset of El Niño. In contrast, the decaying BLT occurs from Feb(1) to Mar(1), which is earlier than observed because the ILD increases in the central Pacific, whereas the MLD varies less than that observed.

3.4. *Factors contributing to interannual BLT variability*

Based on the above analyses, we next analyzed the relationships of the interannual spatiotemporal evolution among the SSS, SST and BLT in the equatorial Pacific. As mentioned above, a BL can occur between the base of the ML and the bottom of the IL due to salinity stratification. Variations in BLT are modulated by variations of both SSS and SST, and the methods of Zhang and Busalacchi (2009) and Zheng et al. (2014) were used to further qualitatively evaluate the factors contributing to the interannual BLT variability. To clearly demonstrate the individual effects of salinity and temperature on BLT, four BLT calculations were performed (Table 1).

3.4.1. *Horizontal distribution*

As shown in Fig. 7, it is evident that the salinity interannual anomaly contributes significantly to the BLT interannual variability around the date line in the western-central Pacific, whereas the temperature anomaly is the major contributor to BLT in the eastern equatorial Pacific through its main effect

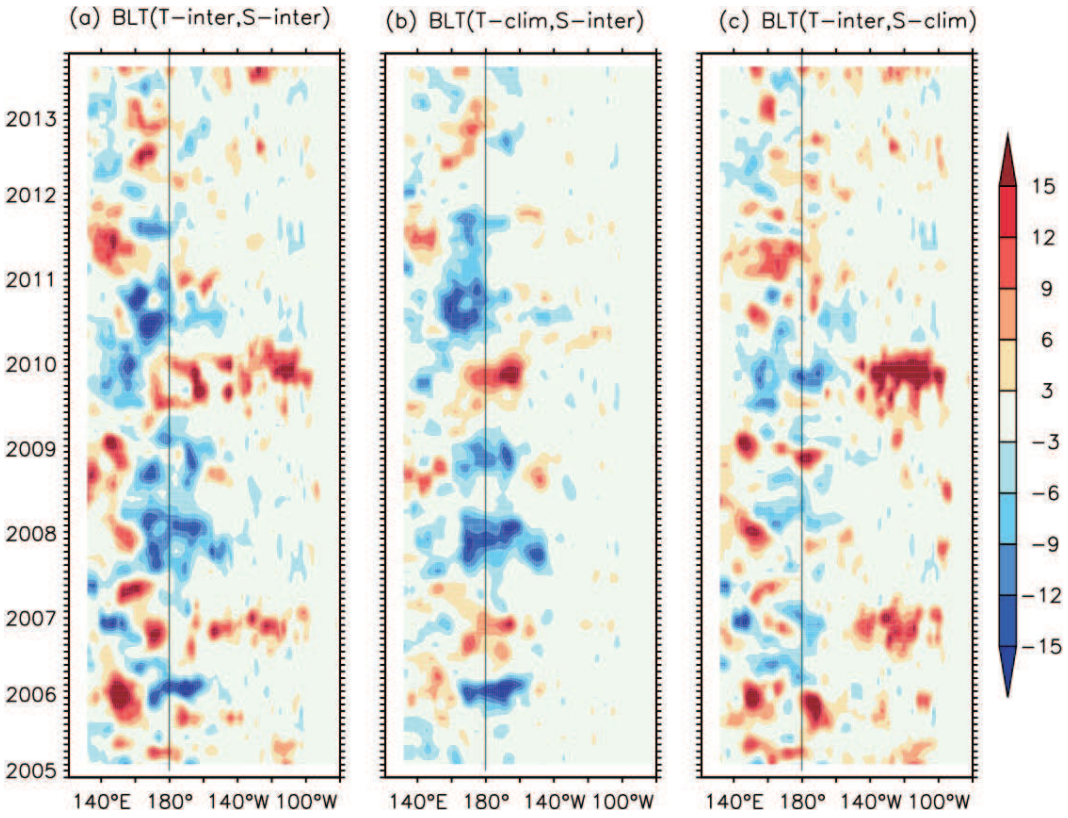

Fig. 7. Longitude–time sections along the equator (averaged from 2°N to 2°S) for the diagnosed BLT from ARGO for (a) ($T_{\text{inter}}, S_{\text{inter}}$), (b) ($T_{\text{clim}}, S_{\text{inter}}$), and (c) ($T_{\text{inter}}, S_{\text{clim}}$).

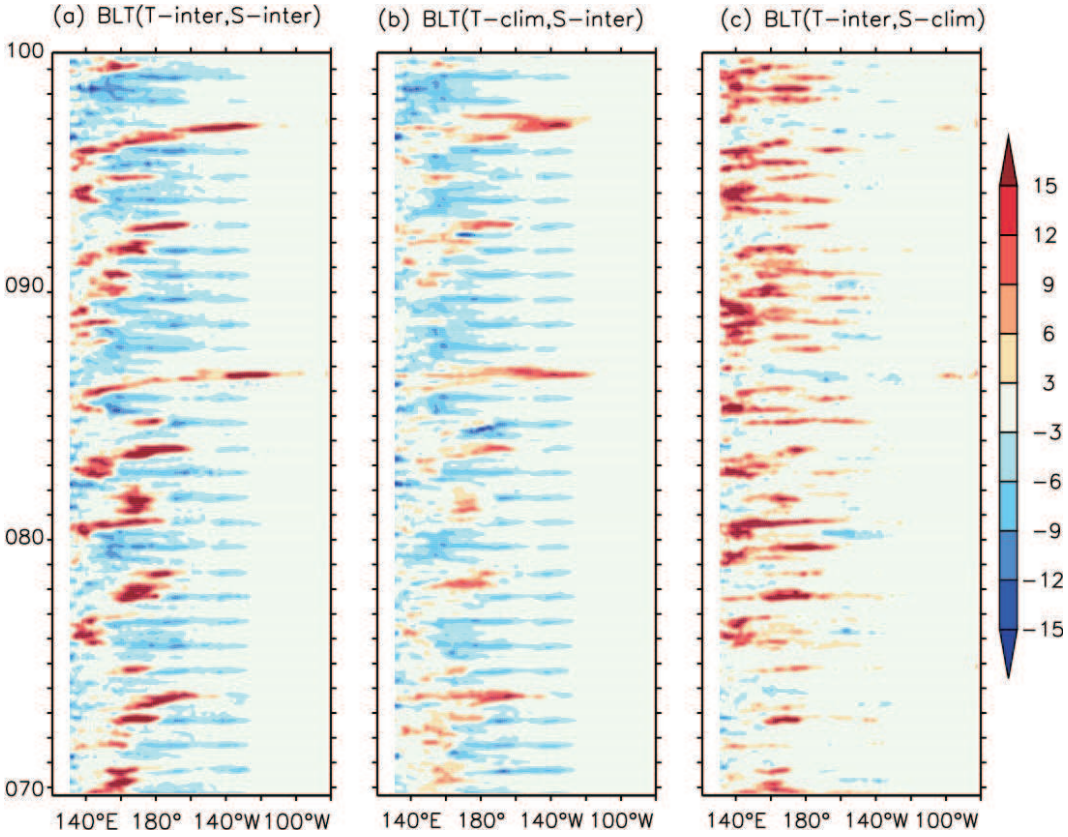

Fig. 8. As in Fig. 7 but for the diagnosed BLT simulated by BNU-ESM. The y-coordinates are the last 30 years of 100 model years.

on the ILD. The observations shown in Fig. 7a indicate that, during the 2010 El Niño, the strong shoaling of the BL was largely due to the effects of positive salinity anomalies in the central basin, as well as positive temperature anomalies in the eastern equatorial region. In fact, similar results were obtained when the BLT was calculated in a manner similar to that previously mentioned, e.g., Zheng et al. (2014).

The same diagnostic steps were used to assess the simulated effect of salinity on the BLT. As shown in Fig. 8, BNU-ESM can reproduce the BLT feature in the equatorial Pacific, whereas the BLT interannual variability is significantly impacted by the interannual anomalies of salinity around the date line in the central basin. This illustrates that, during ENSO, a stronger positive/negative BLT variability corresponds to a strong positive/negative BLT of the interannual salinity anomaly in the western-central Pacific simulated by BNU-ESM. In contrast to observations, the effect of the temperature anomaly on the BLT appears mainly in the eastern equatorial Pacific; whereas, in the model, this effect appears mainly in the western equatorial Pacific. In addition, a BLT related to the salinity anomaly is the major negative contributor to the BLT in the eastern equatorial Pacific through its dominant effect on shoaling the ILD. The location and frequency of positive BLT variability on temperature anomalies are greater than those observed. The reasons for these biases may be that the simulated SSS is stronger than that of the observed SSS in the western Pacific, and that the temperature anomaly results in a stronger interannual MLD variability.

3.4.2. *Vertical stratification*

Finally, the salinity and temperature interannual variability effects on BLT were analyzed and assessed in terms of vertical stratification, in which a dominant factor affecting the MLD variability around the eastern edge of the warm

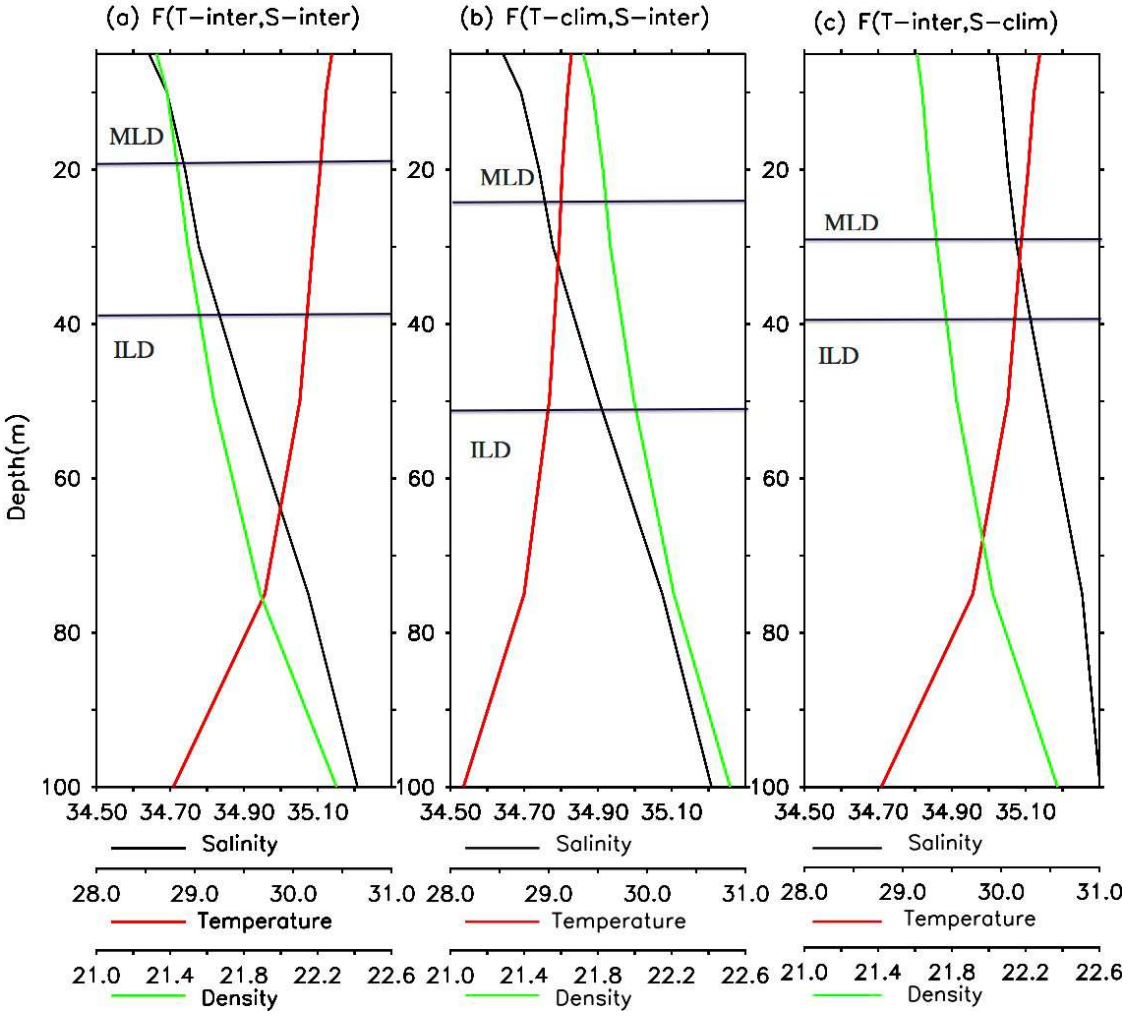

Fig. 9. Vertical profiles of salinity (black line), temperature (red line), density (green line), and the associated MLD, ILD, and BLT in the central equatorial region averaged in the area (2°S–2°N, 175°E–175°W), representing El Niño conditions. Three different diagnostic calculations are compared to illustrate the relative contributions of salinity and temperature to the variations of the MLD, ILD and BLT. The bottoms of the ML and IL are denoted by the black straight lines. The horizontal multi-coordinates represent salinity and temperature, and density at the bottom, respectively. Units are °C for temperature, psu for salinity, kg m^{-3} for density, and m for the MLD, ILD and BLT.

pool can be found. Thus, the effects of salinity interannual variability on the BLT are obviously larger than those of the temperature associated with El Niño conditions in the region. The analyses distinguished the relative contributions of temperature and salinity to the varying BLT anomaly fields in the vertical profile. As shown in Fig. 9, a thicker BL (Fig. 9a, ∼19 m) occurs in association with salinity and temperature anomalies, similar to the BLT pattern (Fig. 9b, ∼28 m) affected by a salinity anomaly, whereas a thinner BLT (Fig. 9c, ∼10 m) appears under the major influence of a temperature anomaly during El Niño. These three cases make it clear that salinity change is a dominant factor affecting BLT variability around the eastern edge of the warm pool in the central basin. Note that the interannually varying temperature is a factor that contributes to BLT variations, which negatively correlate to local SST. The same analyses were applied to the simulation (Fig. 10). However, because the MLDs and ILDs simulated by BNU-ESM are usually shallower than the three observed cases, the BLTs are thinner and shallower than observed in terms of their ocean depth profile during El Niño, especially in an anomalous temperature condition. This result demonstrates that BNU-ESM-simulated BLT is more sensitive to SSS variability and that a large BLT interannual variation is located toward the west of the SSS front.

4. Summary and conclusion

The salinity effects on ocean physics in the western equatorial Pacific are of primary importance to the climate system given the role of salinity in the stratification of the ocean and in ENSO variability. Among numerous atmospheric and oceanic processes that affect SST variability, BL occurrence is clearly of great interest. Present studies illustrate how BL formation is a key mechanism in establishing interannual variability in the equatorial Pacific, and further demonstrate the impact of the coupled system on SST anomalies (Maes et al., 2005; Ando and Hasegawa, 2009). It is important that coupled models, including CMIP5 models, have the capability to reproduce the effect of salinity on SST, and determine the potential resulting BL. It is expected that CMIP5 multimodels can provide realistic ocean simulations and thus improve our knowledge of both the BL and its relationship with ENSO.

In terms of the role of the salinity and its relevance to the dynamics of the BL simulated by BNU-ESM, the present

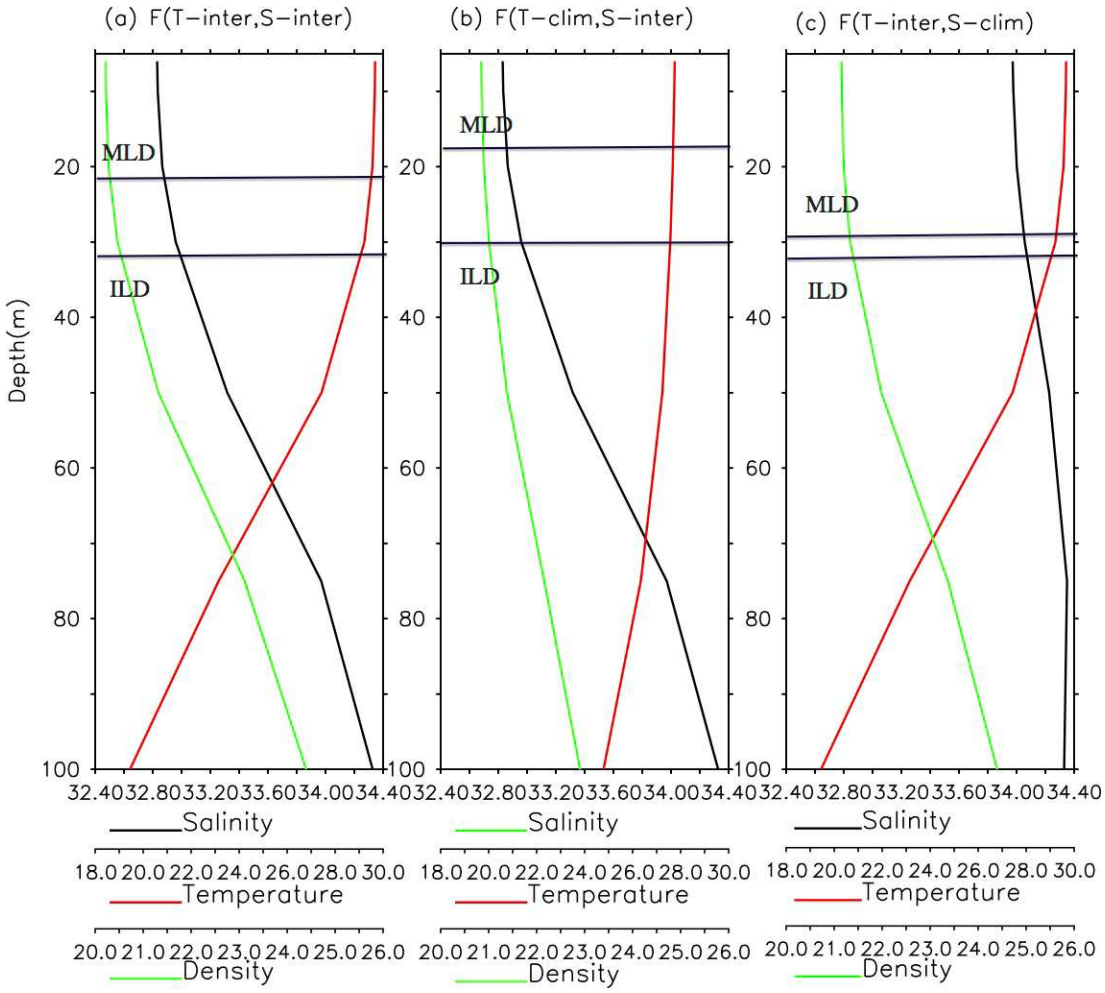

Fig. 10. As in Fig. 9 but for the results simulated by BNU-ESM.

assessment illustrates that the haline stratification in the western Pacific agrees with observations. BNU-ESM can provide realistic descriptions of SSS and BL interannual variability in the equatorial Pacific. Its simulations further demonstrate the observed relationships among the interannual variabilities of salinity, temperature, and BLT, in which salinity plays a key role in SST through stratification. For example, BNU-ESM effectively and realistically reproduces the evolving features of the BLT, MLD and ILD interannual anomalies and their relationships with SSS during El Niño, such as the large variabilities that move back and forth across the SSS front along equator. BNU-ESM can reproduce the indirect feedback from the salinity variations to SST through their role in the stratification of the upper ocean. It is confirmed that the trapping of heat and momentum resulting from salinity-stratified MLs in the western-central Pacific is sufficient to modify the SST balance (Maes et al., 2002, 2005). Additionally, the SSS anomalies simulated by BNU-ESM indicate equatorward migration of the BLs formed off the equator in the Intertropical convergence zone (ITCZ) or the Southern Pacific convergence zone (SPCZ). The BNU-ESM simulation confirms the conclusion discussed in Zheng et al. (2014), with interannual salinity anomalies tending to enhance the interannual variability of the BL while the interannually varying temperature field acting to decrease the BLT variability in this region. So, the salinity and temperature effects tend to partially compensate for each other.

There are obvious biases in BNU-ESM relative to observations in terms of salinity simulation. Due to the higher than observed SSS interannual variability simulated by BNU-ESM in the western equatorial Pacific, the SSS front moves eastward, and a large BLT forms in the western equatorial Pacific and moves eastward in Feb(0), two months earlier than observed. However, the large BLT lasts approximately three months, much shorter than in observations of the El Niño developing phase.

Comparisons between the BNU-ESM simulations and observations indicate that the effect of salinity on the BLT depends on the magnitude of the salinity interannual anomaly simulated by BNU-ESM, which is sensitive to horizontal and vertical displacements along the equator in the central Pacific. The location and frequency of positive BLT variability simulated by BNU-ESM are different from those observed. The reasons for these biases may be that the SSS simulated by BNU-ESM is stronger than the observed SSS in the western Pacific; thus, the temperature anomaly results in a stronger interannual MLD variability. However, because simulated MLDs and ILDs are usually shallower than in the three observed cases of salinity and temperature anomalies, the BLTs are thinner and shallower than those observed in the ocean depth profile during El Niño, especially in anomalous temperature conditions. This result shows that BLTs simulated by BNU-ESM are more sensitive to SSS variability and that significant BLT interannual variation is robustly located toward the west of the SSS front.

Acknowledgements. We thank the modeling groups participating in CMIP5 and PCMDI for generously making available the model outputs used in this paper. This study was supported by the National Natural Science Foundation of China (Grant Nos. 41376039, 41376019 and 41421005), the NSFC-Shandong Joint Fund for Marine Science Research Centers (Grant No. U1406401), and the IOCAS through the CAS Strategic Priority Project [the Western Pacific Ocean System (WPOS)], and the WPOS in the "Strategic Priority Research Program" of the Chinese Academy of Sciences (Grant No. XDA11010304). This is publication No. 074 of the Earth System Modeling Center (ESMC), and the Priority Academic Program Development (PAPD) of Jiangsu Higher Education Institutions.

REFERENCES

AchutaRao, K., and K. R. Sperber, 2006: ENSO simulation in coupled ocean-atmosphere models: Are the current models better? *Climate Dyn.*, **27**, 1–15.

Ando, K., and T. Hasegawa, 2009: Annual zonal displacement of Pacific warm pool in association with El Niño onset. *SOLA*, **5**, 149–152.

Bellenger, H., E. Guilyardi, J. Leloup, M. Lengaigne, and J. Vialard, 2014: ENSO representation in climate models: from CMIP3 to CMIP5. *Climate Dyn.*, **42**, 1999–2018.

Bosc, C., T. Delcroix, and C. Maes, 2009: Barrier layer variability in the western Pacific warm pool from 2000 to 2007. *J. Geophys. Res.* (*Oceans*), **114**, C06023, doi: 10.1029/2008JC 005187.

Brown, J. N., C. Langlais, and C. Maes, 2014: Zonal structure and variability of the Western Pacific dynamic warm pool edge in CMIP5. *Climate Dyn.*, **42**(11–12), 3061–3076.

de Boyer Montégut, C., G. Madec, A. S. Fischer, A. Lazar, and D. Iudicone, 2004: Mixed layer depth over the global ocean: An examination of profile data and a profile-based climatology. *J. Geophys. Res.*, **109**, C12003, doi: 10.1029/2004JC002378.

Delcroix, T., and J. Picaut, 1998: Zonal displacement of the western equatorial Pacific "fresh pool". *J. Geophys. Res.*, **103**, 1087–1098.

Delcroix, T., G. Alory, S. Cravatte, T. Corrège, and M. McPhaden, 2011: A gridded sea surface salinity data set for the tropical Pacific with sample applications (1950–2008). *Deep-Sea Res.*, Part I, **58**, 38–48.

Gill, A. E., 1982: *Atmosphere–Ocean Dynamics*. Academic Press, 662 pp.

Godfrey, J. S., and Coauthors, 1995: The role of the Indian Ocean in the global climate system: recommendations regarding the global ocean observing system. Report of the Ocean Observing System Development Panel, Report No. 6, Texas A&M University, College Station, Texas, 89 pp.

Guilyardi, E., P. Braconnot, F. F. Jin, S. T. Kim, M. Kolasinski, T. Li, and I. Musat, 2009: Atmosphere feedbacks during ENSO in a coupled GCM with a modified atmospheric convection scheme. *J. Climate*, **22**, 5698–5718.

IPCC, 2013: *Climate Change 2013: The Physical Science Basis. Contribution of Working Group I to the Fifth Assessment Report of the Intergovernmental Panel on Climate Change*, T. F. Stocker et al., Eds., Cambridge University Press, Cambridge, United Kingdom and New York, NY, USA, 1535 pp.

Ji, D., and Coauthors, 2014: Description and basic evaluation of BNU-ESM version1. *Geoscientific-Model Dev-Discuss*, **7**,

1601–1647.

Levitus, S., 1982: Climatological atlas of the world ocean. NOAA Prof. Pap. 13, 173, U.S. Gov. Print. Off., Washington, D. C.

Lindstrom, E., R. Lukas, R. Fine, E. Firing, S. Godfrey, G. Meyers, and M. Tsuchiya, 1987: The western equatorial Pacific Ocean circulation study. *Nature*, **330**, 533–537.

Lukas, R., and E. Lindstrom, 1991: The mixed layer of the western equatorial Pacific Ocean. *J. Geophys. Res.*, **96**, 3343–3357.

Maes, C., M. J. McPhaden, D. Behringer, 2002: Signatures of salinity variability in tropical Pacific Ocean dynamic height anomalies. *J. Geophys. Res.*, **107**(C12), 8012, doi: 10.1029/2000JC000737.

Maes, C., J. Picaut, and S. Belamari, 2005: Importance of the salinity barrier layer for the buildup of El Niño. *J. Climate*, **18**(1), 104–118.

Maes, C., K. Ando, T. Delcroix, W. S. Kessler, M. J. McPhaden, and D. Roemmich, 2006: Observed correlation of surface salinity, temperature and barrier layer at the eastern edge of the western Pacific warm pool. *Geophys. Res. Lett.*, **33**(6), L06601, doi: 10.1029/2005GL024772.

Maes, C., and S. Belamari, 2011: On the impact of salinity barrier layer on the Pacific Ocean mean state and ENSO. *SOLA*, **7**(655), 97–100.

Masson, S., J.-P. Boulanger, C. Menkes, P. Delecluse, and T. Yamagata, 2004: Impact of salinity on the 1997 Indian Ocean dipole event in a numerical experiment. *J. Geophys. Res.*, **109**, C02002, doi: 10.1029/2003JC001807.

McPhaden, M. J., and J. Picaut, 1990: El Niño-Southern oscillation displacements of the western equatorial Pacific warm pool. *Science*, **250**, 1385–1388.

Mignot, J., C. de Boyer Montégut, and M. Tomczak, 2009: On the porosity of barrier layers. *Ocean Science*, **5**, 379–387.

Picaut, J., M. Ioualalen, C. Menkes, T. Delcroix, and M. J.McPhaden, 1996: Mechanism of the zonal displacements of the Pacific warm pool: Implications for ENSO. *Science*, **274**, 1486–1489, doi: 10.1126/science.274.5292.1486.

Rao, R. R., and R. Sivakumar, 2003: Seasonal variability of sea surface salinity and salt budget of the mixed layer of the north Indian Ocean. *J. Geophys. Res.*, **108**(C1), 3009, doi: 10.1029/2001JC000907.

Roemmich, D., and Coauthors, 2009: The Argo Program: Observing the global ocean with profiling floats. *Oceanography*, **22**, 34–43.

Sato, K., T. Suga, and K. Hanawa, 2006: Barrier layer in the subtropical gyres of the world's oceans. *Geophys. Res. Lett.*, **33**, L08603, doi: 10.1029/2005GL025631.

Sprintall, J., and M. Tomczak, 1992: Evidence of the barrier layer in the surface layer of the tropics. *J. Geophys. Res.*, **97**, 7305–7316.

Stoens, A., and Coauthors, 1999: The coupled physical new production system in the equatorial Pacific during the 1992–1995 El Niño. *J. Geophys. Res.*, **104**, 3323–3339.

Su, H., and J. H. Jiang, 2012: Tropical clouds and circulation changes during the 2006/07 and 2009/10 El Niños. *J. Clim*ate, **26**, 399–413, doi: 10.1175/JCLI-D-12-00152.1.

Taylor, K. E., R. J. Stouffer, and G. A. Meehl, 2012: An overview of CMIP5 and the experiment design. *Bull. Amer. Meteor. Soc.*, **93**, 485–498.

Vannière, B., E. Guilyardi, G. Madec, F. J. Doblas-Reyes, and S. Woolnough, 2011: Using seasonal hindcasts to understand the origin of the equatorial cold tongue bias in CGCMs and its impact on ENSO. *Climate Dyn.*, **40**, 963–981.

Vialard, J., and P. Delecluse, 1998: An OGCM study for the TOGA decade: II. Barrier-layer formation and variability. *J. Phys. Oceanogr.*, **28**, 1089–1106.

Yim, B. Y., S.-W. Yeh, Y. Noh, B.-K. Moon, and Y.-G. Park, 2008: Sea surface salinity variability and its relation to El Niño in a CGCM. *Asia-Pacific J. Atmos. Sci.*, **44**(2), 173–189.

Yu, J. Y., and S. T. Kim, 2011: Reversed spatial asymmetries between El Niño and La Niña and their linkage to decadal ENSO modulation in CMIP3 models. *J. Climate*, **24**, 5423–5434.

Yu, J. Y., and S. T. Kim, 2010: Identification of central-Pacific and Eastern-Pacific types of ENSO in CMIP3 models. *Geophys. Res. Lett.*, **37**, L15705, doi: 10.1029/2010GL044082.

Zhang, R. H., and A. J. Busalacchi, 2009: Freshwater flux (FWF)-induced oceanic feedback in a hybrid coupled model of the tropical Pacific. *J. Climate*, **22**, 853–879.

Zhang, R. H., G. H. Wang, D. K. Chen, A. J. Busalacchi, and E. C. Hackert, 2010: Interannual biases induced by freshwater flux and coupled feedback in the tropical Pacific. *Mon. Wea. Rev.*, **138**, 1715–1737.

Zhang, R. H., S. E. Zebiak, R. Kleeman, and N. Keenlyside, 2005: Retrospective El Niño forecasts using an improved intermediate coupled model. *Mon. Wea. Rev.*, **133**, 2777–2802.

Zheng, F., and R. H. Zhang, 2012: Effects of interannual salinity variability and freshwater flux forcing on the development of the 2007/08 La Niña event diagnosed from Argo and satellite data. *Dyn. Atmos. Oceans*, **57**, 45–57.

Zheng, F., and R. H. Zhang, 2015: Interannually varying salinity effects on ENSO in the tropical Pacific: A diagnostic analysis from Argo. *Ocean Dynamics*, **65**(5), 691–705.

Zheng, F., R. H. Zhang, and J. Zhu, 2014: Effects of interannual salinity variability on the barrier layer in the western-central equatorial Pacific: A diagnostic analysis from Argo. *Adv. Atmos. Sci.*, **31**(3), 532–542, doi: 10.1007/s00376-013-3061-8.

Zheng, F., H. Wang, and L. Y. Wan, 2015: Effects of interannual salinity variability on the dynamic height in the western equatorial Pacific as diagnosed by Argo. *Acta Oceanologica Sinica*, **34**(5), 22–28.

Zhi, H., R. H. Zhang, P. F. Lin, and L. N. Wang, 2015: Simulation of salinity variability and the related freshwater flux forcing in the tropical pacific: An evaluation using the Beijing Normal University Earth System Model (BNU-ESM). *Adv. Atmos. Sci.*, **32**, 1551–1564, doi: 10.1007/s00376-015-4240-6.

Zhu, J. S., G. Q. Zhou, R. H. Zhang, and Z. B. Sun, 2013: Improving ENSO prediction in a hybrid coupled model with an embedded entrainment temperature parameterisation. *Int. J. Climatol.*, **33**(2), 343–355.

Zhu, J. S., B. H. Huang, R. H. Zhang, Z. Z. Hu, A. Kumar, M. A. Balmaseda, L. Marx, and J. L. Kinter III, 2014: Salinity anomaly as a trigger for ENSO events. *Sci. Rep.*, **4**, 6821, doi: 10.1038/srep06821.